The effect of hydrogen on the crack initiation site of TRIP-assisted steels during in-situ hydrogen plasma micro-tensile testing: leading to an improved ductility?

T. Depover[1], D. Wan[2], D. Wang[2], A. Barnoush[2] and K. Verbeken[1]

[1]*Department of Materials, Textiles and Chemical Engineering, Ghent University (UGent), Technologiepark 46, B-9052 Ghent, Belgium*

[2]*Department of Mechanical and Industrial Engineering, Norwegian University of Science and Technology (NTNU), Richard Birkelands vei 2, 7491 Trondheim, Norway*

Corresponding author:
Tom Depover
E-mail: Tom.Depover@ugent.be

Keywords: Environmental assisted cracking; Tensile testing; Microstructure; Thermal Desorption Spectroscopy; Scanning electron microscopy; Crack initiation

Abstract

The hydrogen induced damage and crack initiation in transformation induced plasticity (TRIP) steel is considered in the present work by micro tensile testing and subsequent microstructural assessment. Hydrogen characteristics are studied for two material conditions for this purpose, i.e. TRIP 0% and TRIP 15%. To increase, on the one hand, microstructural defects such as dislocations, and on the other hand, to provoke the strain induced phase transformation of retained austenite to fresh martensite, cold deformation of 15% is applied (TRIP 15%) and compared to the as-received material (TRIP 0%). Both electrochemical charging and hydrogen plasma charging is done compared to uncharged tensile specimens, as reference. A hydrogen induced ductility loss is found when the samples are hydrogen charged electrochemically, whereas plasma charging remarkably induces a ductility increase. A comprehensive hydrogen assisted crack analysis by environmental scanning electron microscopy reveals that the uncharged and electrochemically charged specimens show crack initiation in the martensitic regions, whereas plasma charging results into crack initiation in the soft, crack arresting ferritic matrix. Furthermore, the hydrogen effect is for both charging methods more pronounced after cold deformation, which is correlated to hydrogen trapping ability of the deformation induced defects, as verified by thermal desorption spectroscopy.

1. Introduction

Hydrogen embrittlement is a severe type of environmental assisted cracking affecting most metals and their alloys. Specifically, a degradation of the materials' performance, resulting in ductility loss, unpredictable failure or delayed cracking, is observed. Even though numerous researchers have investigated the consequences of the hydrogen presence [1, 2, 3, 4, 5], still no comprehensive fundamental understanding of the mechanism behind has been established. Therefore, further insight on the hydrogen/material interaction is of crucial importance since the relevance of the hydrogen economy has recently resulted in significantly more attention in this topic. As an eco-

friendly energy carrier, hydrogen may indeed enable an energy revolution towards renewable and sustainable energy systems [6]. Major challenge for the future is the storage of energy. Green power production is expected to significantly increase over the coming years. This will include high fluctuations between supply and demand, which can be responded by converting the surplus electricity into hydrogen; the excess green energy coming from solar and wind energy can be converted into hydrogen gas. As such, it can be stored in the existing gas grid or in salt caverns, potentially replacing natural gas for energy supply to housing, industry and transport. Major efforts into the hydrogen economy are ongoing in countries as the Netherlands, UK, Japan, Norway, etc [6, 7, 8].

In other effort to build a sustainable economy and to reduce pollutant CO_2 emissions, the use of advanced high-strength steels is required for lightweight assembly and therefore improved fuel efficiency to reduce the energy consumption. Although materials with outstanding combinations of high strength levels with high fracture toughness have been developed, hydrogen embrittlement is still a major concern for their application as the fracture resistance is considerably reduced by hydrogen. The automotive industry, for instance, encounters these issues challenging future alloy development [9]. Transformation induced plasticity (TRIP), dual phase (DP), high strength low alloy (HSLA) and martensitic steels are the main grades within this advanced high strength steels category. Depover et al. [3, 10] evaluated their vulnerability to hydrogen by in-situ tensile testing. HSLA displayed a high hydrogen embrittlement resistance, for which the presence of carbides was set responsible. On the contrary, DP and TRIP steel embrittled significantly (> 50% ductility loss). Laureys et al. [11, 12, 13] studied this specific TRIP steel in more detail. They performed similar in-situ tensile tests on notched specimen and interrupted them to assess the hydrogen assisted crack initiation and propagation pathway. The governing mechanism for hydrogen crack initiation was found to be decohesion of the martensite/martensite interface, following the hydrogen enhanced interface decohesion (HEIDE) mechanism. Further crack propagation followed two steps. At first, the initiated cracks grew and, secondly, coalescence of small cracks took place, causing stepwise cracking. When the crack is propagating in ferrite, the hydrogen enhanced localized plasticity (HELP) mechanism appears to act, since the present crack tips were surrounded by high strain fields, as verified by electron backscatter diffraction (EBSD). However, the crack tip follows the martensite/matrix interface in the vicinity of martensitic regions, leading to interface decohesion. Thus, both HELP and HEIDE are active in these TRIP-assisted steels [11, 12].

These TRIP steels are low carbon steels presenting a transformation induced plasticity effect. The typical microstructure consists of ferrite, bainite, martensite and metastable retained austenite (γ). The latter plays a crucial role upon deformation, accounting for the specific characteristics of this steel type. Retained austenite transforms into martensite upon straining, which causes an enhanced strain hardening and therefore a good combination of tensile strength and fracture toughness [14]. Nevertheless, all mentioned microstructural constituents show a particular interaction with hydrogen. For instance, the diffusivity and solubility of hydrogen significantly differs between ferrite and austenite due to their crystal structures, i.e. body centered cubic (bcc) and face centered cubic (fcc), respectively [15]. Furthermore, martensite shows a hydrogen diffusivity lying in between ferrite and austenite [16, 17]. Since the ductility of TRIP steels is partially based on the strain induced transformation of retained austenite into martensite, their interaction with hydrogen is of key importance. Due to its low hydrogen diffusivity and high hydrogen solubility, austenite may act as a hydrogen reservoir. Pérez Escobar et al. [18] performed thermal desorption spectroscopy (TDS) on the TRIP-assisted grade studied in this work to evaluate the available trapping sites. They revealed that the retained austenite fraction contained hydrogen, originating from the processing of the material, more specifically from the intercritical annealing process. This metastable, hydrogen

containing, austenite will transform to martensite upon straining resulting in hydrogen supersaturated martensite. Recently, Claeys et al. [19] observed for the first time by EBSD that the presence of hydrogen even encourages this martensitic transformation during straining of duplex (austenite/ferrite) stainless steel. Both ε- and α'-martensite was detected in the austenite phase of the hydrogen charged specimens, while martensite was absent for the uncharged specimens. This was explained by a reduction in stacking fault energy (SFE) accompanied with a shift in which phase accommodates most of the plastic deformation. The pinning of edge dislocations by hydrogen atmospheres inhibiting cross-slip also contributed to the shift in the observed deformation mechanism for the hydrogen charged and uncharged material. Moreover, Wang et al. [20] also recently observed martensitic transformations in an interstitial metastable high-entropy alloy during cathodic hydrogen charging, where a critical amount of hydrogen was found to be required to induce the phase transformation from γ to ε-martensite. Furthermore, McCoy and Gerberich [21] claimed that TRIP-assisted steel is quite resistant to hydrogen in the austenitic state, whereas it was again confirmed that the strain-induced martensite showed embrittlement due to hydrogen. Chan [22] further proved that fresh martensite is very prone to hydrogen damage since the lath martensite has a large density of dislocations and residual micro-stresses. The actual deformation mechanism of TRIP comprises a displacive transformation which, on the one hand, transforms the hydrogen containing austenitic phase into a severely hydrogen embrittlement prone martensitic phase containing a reduced solubility for hydrogen. However, on the other hand, also crystallographic defects and internal stresses are generated during the deformation, affecting the hydrogen assisted cracking [23, 24, 25, 26]. Consequently, the impact of hydrogen in TRIP-assisted steels has, due to its complex microstructure, still not been fully understood.

Different procedures to charge a certain material with hydrogen have been used over the years to study the change in the material's mechanical properties due to the presence of hydrogen. Mainly electrochemical charging [27, 28, 29, 30, 31] and gaseous charging [32, 33, 34, 35] are used to induce hydrogen into the material of interest. Recently, a novel plasma charging technique was developed to evaluate hydrogen embrittlement, where tensile tests were done together with hydrogen plasma charging inside an environmental scanning electron microscope (ESEM) [36]. Another study [37] further compared this in-situ plasma charging method with conventional electrochemical charging in DP steel and found very similar observations for both charging procedures, endorsing plasma charging as a reliable technique to evaluate the hydrogen effect on the mechanical properties. In addition, in-situ hydrogen charging has proven to be essential to evaluate the hydrogen characteristics due to the high hydrogen fugacity in bcc steels [23, 38]. Up to now, in-situ charging was either done by hydrogen gas or electrochemical cathodic charging. Both methods cannot provide high-resolution observation of the sample during deformation due to the experimental constraints. In-situ hydrogen plasma charging offers opportunities for an ESEM observation subsequent to tensile testing, which is an important asset.

The goal of this research is to examine the hydrogen assisted crack initiation and mechanical behavior of TRIP steel by in-situ hydrogen plasma charging. The established methodology from Refs. [36, 37] will be used hereto. Plasma charging will be compared with conventional electrochemical cathodic charging and both will be compared with reference tensile tests performed without hydrogen charging. The hydrogen assisted crack formation will be analyzed by ESEM imaging, aiming at revealing the impact of the different hydrogen charging procedures on the fracture development. Furthermore, cold deformation is applied on the as-received material to induce, on the one hand, an increase in dislocation density and, on the other hand, a strain induced transformation from retained austenite to martensite. As such, their role on the hydrogen embrittlement characteristics can be evaluated.

2. Experimental procedure

This work examines the susceptibility to hydrogen induced mechanical degradation of TRIP-assisted steel by tensile testing and the hydrogen assisted crack pathway by ESEM microstructural evaluation. Hot and cold rolling was done till a thickness of 0.7 mm, subsequently followed by annealing via industrial annealing parameters to attain the desired ferrite-martensite-bainite-retained austenite multiphase microstructure. The chemical composition of the present TRIP-steel is presented in Table 1. Deformation of 15% in thickness was applied by cold rolling to increase the density of deformation induced microstructural defects (i.e. dislocations) and to provoke the strain induced phase transformation from retained austenite to fresh martensite. Consequently, two different material conditions were compared for this TRIP grade: the as-received materials, termed "TRIP 0%", and the cold deformed condition, termed "TRIP 15%".

EBSD was done to assess the degree of the deformation induced phase transformation and to attain a quantitative indication on the increase in dislocation density induced the applied cold deformation. For this purpose, samples were first polished (up to 1 μm), followed by an additional step using colloidal silica (Struers OPU suspension). Measurements were executed on the transversal direction (TD)-plane for which a SEM (FEI Quanta 450) with field emission gun was employed at an acceleration voltage of 20 kV, emission current of 200 μA, specimen tilt of 70° and a scan step size of 80 nm on a hexagonal scan grid. The geometrically necessary dislocation (GND) density was determined by the TSL-OIM Data Analysis V7 software. This density was calculated using local misorientations below 5° and a second neighbor misorientation averaging, for which a clean-up of neighbor confidence index correlation was done. The confidence index quantifies the trustworthiness of the indexation pattern, for which the minimum was set at 0.1.

Table 1: Chemical composition of TRIP-assisted (wt%).

Fe	C	Mn	Si	Other
Balance	0.17	1.60	0.40	1%-2% Al, 0.04%-0.1% P

Micro-waterjet cutting was used to machine to tensile specimens assuring the tensile axis along the rolling direction. A dog-bone-shaped tensile sample was opted with gauge geometry of 5 x 2 x 0.6 mm^3 (cf. Figure 1). Surfaces and edges got prepared by grinding, followed by diamond paste polishing up to 1 μm. Then, to assure a smooth surface finish without residual deformation, electropolishing was performed. In-situ plasma hydrogen charging was done by a plasma source (Evactron Model 25 Zephyr) with H_2 as process gas. The interaction with the steel happens far from the plasma glow, which prevents the material from heating. A compact tensile device (Kammrath & Weiss GmbH) was implemented inside the ESEM chamber (Quanta 650) to perform the micro-mechanical testing. The experimental setup is presented in Figure 2 [36]. Plasma pre-charging was done for two hours while in-situ plasma charging sustained during the micro-tensile test, for which an engineering strain rate of 10^{-4} s^{-1} was chosen. This rather slow strain rate was preferred to enable hydrogen plasma to further adsorb and diffuse into the steel during tensile testing.

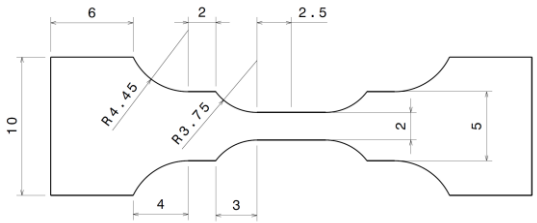

Figure 1: Tensile sample geometry in mm (thickness = 0.6 mm).

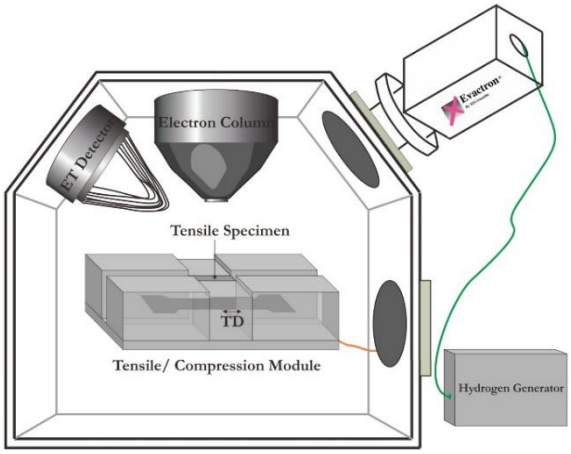

Figure 2: Experimental setup of the SEM chamber (TD: tensile direction) [36].

Besides micro-mechanical tensile testing after and during in-situ hydrogen plasma charging, tensile tests inside the ESEM were also done following conventional electrochemical cathodic hydrogen charging. Successively, thus after the electrochemical charging, the tensile specimens got mounted inside the same ESEM (cf. Figure 2) within 2 minutes. Therefore, hydrogen charging did not continue during the micro-mechanical tensile testing for these electrochemical charged tests. Since plasma charging is a rather innovative charging procedure, the conventional electrochemical charging is added to compare both charging methods. A borax/glycerol based electrolyte was used for the electrochemical charging to eliminate surface contamination/damage, as demonstrated in [39]. A current density of 10 mA/cm^2 for 2 hours was chosen for this purpose. Successively, the tensile specimens got mounted inside the same ESEM within 2 minutes. Both charging methods, i.e. hydrogen plasma and electrochemical cathodic charging, were related to tests done without hydrogen loading (as reference), also executed in the ESEM chamber under the same pressure conditions. Hence, the impact of both charging procedures on the hydrogen embrittlement sensitivity of TRIP-assisted steel can be valued by comparing the determined engineering stress-strain curves with the uncharged (reference) ones. The hydrogen embrittlement (HE) degree was considered by Eq. 1, with ε_{ch} and ε_{un} being the strain at fracture of, respectively, the charged and uncharged tensile specimens.

$$\%HE = 100 \cdot \left(1 - \frac{\varepsilon_{ch}}{\varepsilon_{un}}\right) \tag{1}$$

Next, the hydrogen related characterization was done; at first, the hydrogen content was measured by hot extraction at 300°C to determine the diffusible hydrogen content [23]. Similarly as for the micro-tensile tests, these samples were also tested two minutes after electrochemical hydrogen charging. An infrared furnace is used for this purpose where a pre-weighted sample is heated up to 300°C, where the sample releases its hydrogen as hydrogen gas. This gas is then dragged along a N_2 carrier gas flow and the resulting mixture is sent to a thermal conductivity cell. Due to the conductivity difference of hydrogen and the carrier nitrogen gas, the resulting conductivity depends on the hydrogen content, which can then be computed. Secondly, to identify both the hydrogen trap sites and their related desorption activation energy (E_a), TDS was done as well, for which three different heating rates of 200°C/h, 600°C/h and 1200°C/h were selected. In this case, a mass spectrometer was used as hydrogen gas detector and coupled to the same infrared furnace. Again, similarly as for the tensile tests, samples got analysed two minutes after electrochemical cathodic hydrogen charging. The E_a of the hydrogen traps responsible for the observed TDS spectrum was determined based on the often used work of Lee *et al.* [40]. Eq. 2 denotes a simplified formula of the original one [41], where Φ represents the applied heating rate (K/min), T_{max} (K) the peak temperature, E_a

(J/mol) the detrapping activation energy and R ($JK^{-1}mol^{-1}$) the universal gas constant. All detected spectra were subsequently deconvoluted and the corresponding peak temperatures (T_{max}) for each trap were determined for all heating rates. Finally, the related E_a of that specific considered hydrogen trap can be obtained by plotting $\ln(\Phi/T_{max}^2)$ vs. $(1/T_{max})$.

$$\frac{d(\ln\frac{\Phi}{T_{max}^2})}{d(\frac{1}{T_{max}})} = -\frac{E_a}{R} \quad (2)$$

3. Microstructural characterization

The microstructure of the considered TRIP-assisted steel consists of ferrite, martensite, bainite and retained austenite, as demonstrated in [3]. The amount of retained austenite, quantified by X-ray diffraction (XRD), was determined to be 9.6%, whereas the carbon content of the retained austenite was about 1.2 wt% [18]. Cold deformation by 15% cold rolling resulted in a decrease of the fraction of retained austenite due to its transformation to martensite. This is shown in Figure 3 by the SEM-EBSD phase maps of TRIP 0% and 15%, for which the corresponding inverse pole figure (IPF) maps are given as well. The fraction of retained austenite decreased from 9.6% to 1.8% after 15% cold deformation. Due to the low confidence index of the martensite phase, it was not indexed in the EBSD measurement and is represented by black pixels in the phase maps. The remaining retained austenite fraction in TRIP 15% is also surrounded by the martensitic phase as a result from the deformation induced phase transformation. In addition to the phase transformation, the application of deformation also resulted in an increase in dislocation density. This was evaluated by determining the GND density, as described in the experimental procedure. Only the ferrite phase with CI > 0.1 was considered in this procedure, where the increase in dislocation density is primarily considered. As such, the austenitic, martensitic and bainitic islands were excluded from the GND determination. The results are summarized in Table 2. Cold deformation clearly resulted in an increase in dislocation density in the ferritic grains.

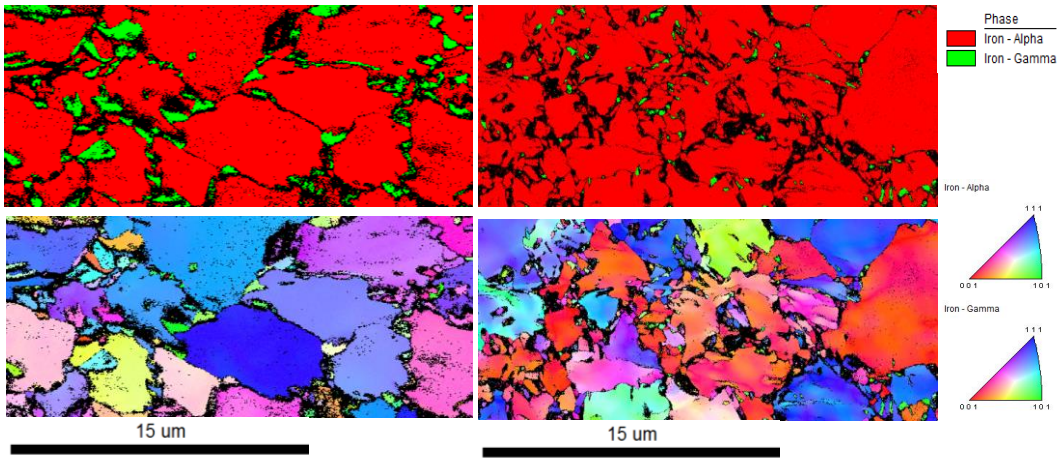

(a) (b)

Figure 3: SEM-EBSD phase maps (top) and inverse pole figure maps (bottom) of TRIP 0% (a) and TRIP 15% (b).

Table 2: Geometrically necessary dislocation density in ferrite of TRIP 0% and TRIP 15%

	GND (10^{12} m^{-2}) in ferrite
TRIP 0%	205
TRIP 15%	272

4. Hydrogen embrittlement sensitivity evaluated by micro-mechanical testing

Two hydrogen charging methods, i.e. plasma and electrochemical charging, were applied on two material conditions (TRIP 0% and TRIP 15%). Both charging methods were compared with uncharged reference tensile samples. The engineering stress-strain curves are depicted in Figure 4 and the resultant hydrogen embrittlement degrees, obtained as described in Eq. 1, are summarized in Table 3. An ultimate tensile stress of about 700 MPa is obtained for TRIP 0% when considering the tests done without hydrogen charging. This is in good agreement with previously reported results on this commercial grade [3]. The yield strength significantly increased when 15% of cold deformation was applied due to strain hardening, together with a considerable decrease of ductility. Both can be linked to the increase in dislocation density, as indicated by GND calculations (cf. Table 2), and the deformation induced phase transformation from austenite to martensite (cf. Figure 3). In addition, the TRIP-effect was also considerably less pronounced for TRIP 15% due to the decreased fraction of retained austenite, i.e. 1.8% vs. 9.6% for TRIP 0%, which remained to transform during the tensile test.

Remarkable results were observed when the materials were charged in-situ with hydrogen plasma for two hours, with plasma charging continuing during the tensile test. A hydrogen induced ductility increase was detected, whereas the strength level increased slightly. A similar though consistently larger impact on both the strength level and ductility was observed for TRIP 15%, demonstrating the reliability of these noteworthy results. Plasma charging was, however, also conducted in earlier work on Fe-3%Si [36] and DP steel [37], where plasma charging resulted, similarly to conventional electrochemical charging, in a hydrogen induced ductility loss. Therefore, these striking results deserve further attention and will be elaborated in more detail below when assessing the crack initiation and propagation in section 6.

Specimens were also charged by conventional electrochemical charging prior to tensile testing to verify the effect of hydrogen on the mechanical properties of this material in this novel test set-up. For these conditions, the anticipated results of hydrogen charging were observed, i.e. the strength level slightly increased while ductility was reduced. This tendency was again more pronounced when cold deformation was applied. The increase of the yield strength can be attributed to solid solution strengthening by hydrogen [42, 43, 44, 45, 46]. A slight hardening due to plasma charging was also observed in [36], while similar effects due to electrochemical hydrogen charging were found in [3, 47]. Based on the obtained degrees of HE, as summarized in Table 3, it was observed that the hydrogen effect was generally more pronounced for TRIP 15%, probably due to the deformation induced defects and their interaction with hydrogen, as will be discussed in the following section when evaluation the trapping ability of these materials by thermal desorption spectroscopy.

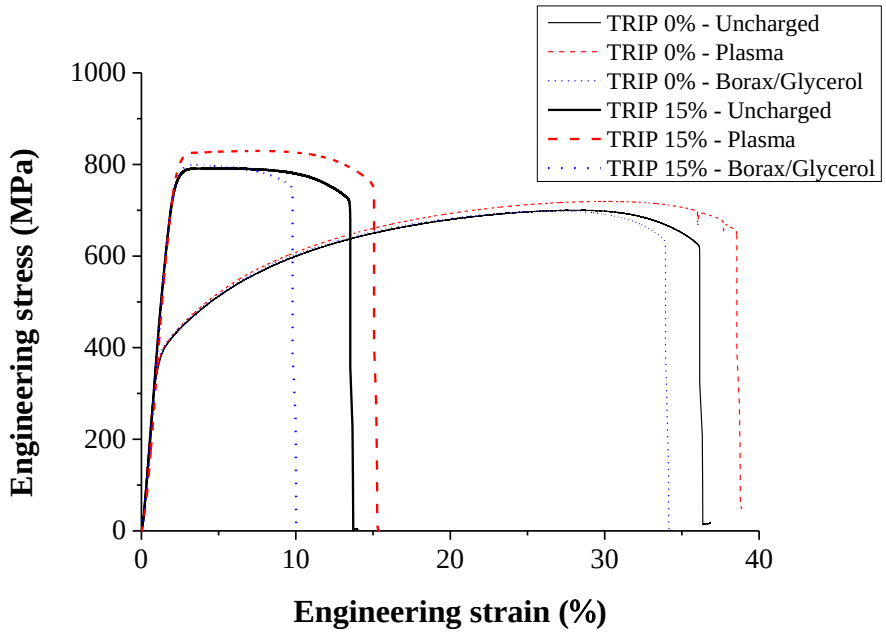

Figure 4: Engineering strain-strain curves of TRIP 0% and TRIP 15% in the uncharged, hydrogen plasma charged and electrochemical charged condition.

Table 3: Summary of the HE% of TRIP 0% and TRIP 15% in the hydrogen plasma and electrochemical charged condition.

HE (%)	Plasma	Borax/Glycerol
TRIP 0%	-7	7
TRIP 15%	-11	27

5. Effect of cold deformation on the hydrogen trapping ability by TDS

Hydrogen trapping was evaluated for the samples charged electrochemically with borax/glycerol electrolyte to determine the available hydrogen trapping sites. Hot extraction was first done to determine the diffusible hydrogen content and showed that that saturation was reached after two hours of charging and that rather low amounts of hydrogen were obtained with this electrolyte (cf. Figure 5 (a)). Furthermore, the reduced HE resistance for TRIP 15% compared to TRIP 0% can also be linked to the higher amount of hydrogen charged in the material. Next to the hydrogen level in the material, also the effective trapping sites play a crucial role to understand the observed HE degrees.

Therefore, TDS was done at three different heating rates and the corresponding spectrum of the heating rate at 600°C/h is shown in Figure 5 (b), for sake of clarity. Firstly, TRIP 15% contained more hydrogen compared to TRIP 0% below 300°C, which is consistent with the hot extraction results done at 300°C (cf. Figure 5 (a)). Secondly, a distinct shoulder at the start of the spectrum (< 100°C) is clearly observed when cold deformation was applied. Only a limited indication of this shoulder is detectable for TRIP 0%. Depover et al. [23] recently correlated this first shoulder in the TDS spectrum to hydrogen trapped by dislocations by varying the amount of deformation. This indicated that the deformation induced defects, such as dislocations, represented by the increase in GND's, were able to trap hydrogen. This particular hydrogen has been confirmed to play a detrimental role in HE. This was associated to the HELP mechanism, which proposes an enhanced dislocation mobility in the presence of

hydrogen [23]. Further, the broad low temperature TDS peak, which is present for both conditions, increased when cold deformation was applied. This was linked to the increased amount of martensite, resulting from the retained austenite transformation, as demonstrated by Pérez Escobar et al. [18].

This TRIP steel also contained a distinct high temperature peak. In the detailed TDS analysis performed by Pérez Escobar et al. [18], it was demonstrated that this peak resulted from hydrogen being trapped by retained austenite. The origin of this hydrogen can be found in the processing of the material rather than in the applied hydrogen charging procedure, as discussed in the introduction of this work. Consequently, the applied deformation resulted in a decrease of the retained austenite fraction, as shown by the phase maps in the EBSD analysis (cf. Figure 3). Moreover, both a shift to lower temperatures as to a lower hydrogen level were detected, which are both a consequence of the decreased retained austenite fraction, as discussed in more detail in the work of Pérez Escobar et al. [18]. In conclusion, hydrogen charging resulted in the lower temperature peaks, whereas the high temperature peaks were already present before hydrogen charging. The amount of hydrogen covered by the low temperature peak (< 300°C) is identical to the one obtained by hot extraction (cf. Figure 5 (a)). The high temperature peaks were not incorporated in the hot extraction analysis at 300°C.

Deconvolution of all TDS spectra in three separate peaks enabled the determination of the corresponding activation energies. Peak 1, represented by the shoulder (< 100°C) and only clearly present for TRIP 15%, shows an E_a of about 25 kJ/mol which corresponds to hydrogen trapped at dislocations [48, 49]. The trapping ability of dislocations by this TDS device has been confirmed in [23]. The second peak, present for both material conditions at low temperature, contains an E_a of about 30 kJ/mol. This can hence be linked to the grain boundaries and martensitic lath boundaries [50, 51, 52]. Finally, the third high temperature peak has an E_a of about 90 kJ/mol and results from hydrogen trapped at retained austenite.

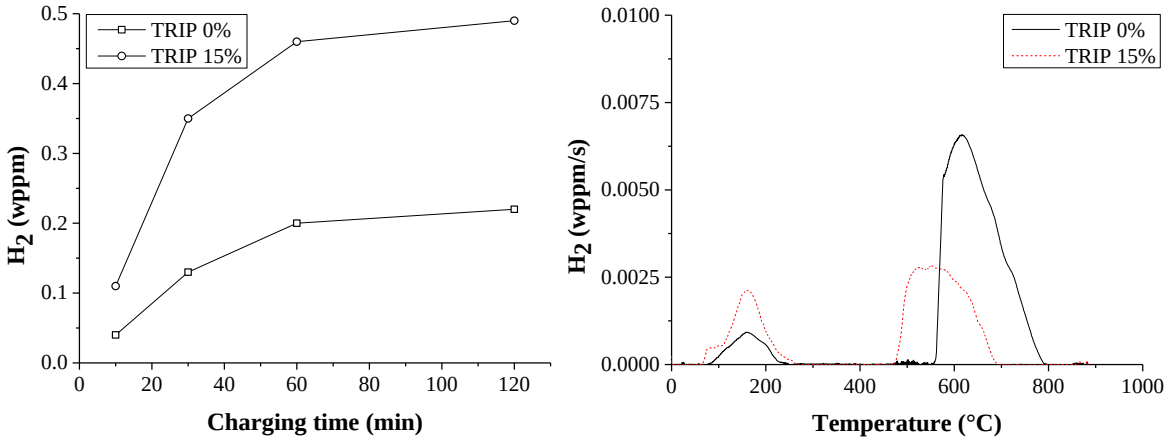

Figure 5: Diffusible hydrogen content (wppm) vs. applied charging time for TRIP 0% and TRIP 15% (a) and TDS spectra at heating rate of 600°C/for TRIP 0% and TRIP 15% h (b).

6. Assessment of the hydrogen assisted crack initiation by SEM

As already shortly stated in the introduction, Laureys et al. [11, 12] demonstrated that electrochemically charged hydrogen did not seem to influence the hydrogen induced crack initiation site in this TRIP steel, as for both the uncharged and hydrogen charged condition, cracks initiated in the martensitic regions. However, the kinetics of further crack propagation in the surrounding matrix were significantly affected by hydrogen charging, since the crack arresting ability of the surrounding ferrite is strongly decreased when charged with hydrogen. Therefore, the advantages of the TRIP effect are lost in the presence of hydrogen, resulting in a significant hydrogen induced ductility loss. To further understand the obtained HE degrees in the present work (cf. Table 3), especially the noteworthy results for plasma charging, the crack initiation site was further evaluated by ESEM analysis. Note that no additional sample preparation was required since the tensile tests were performed inside the ESEM chamber, which enables a direct observation whenever essential to comprehend crack formation. Detailed ESEM images for the three considered environments, i.e. uncharged, electrochemical and plasma, of both material conditions are shown in Figure 6, mainly focusing on the crack initiation point. These initiating cracks were mainly observed from necking onwards. The ESEM images were taken on the ND-plane after final fracture.

At first, the electrochemical hydrogen charging condition is considered and compared to the reference uncharged tensile tests. Crack initiations occurred in, along or in between martensitic regions for both conditions, as illustrated in Figure 6. In this figure, the crack initiation site has been indicated by the white arrows. These images are representative and based on ten SEM images per condition to guarantee the statical reliability. This is associated to the hydrogen containing retained austenite which is transforming into fresh martensite upon tensile testing. This transformation induced martensite is supersaturated with hydrogen since it originates from hydrogen containing retained austenite (cf. TDS results). This martensite and especially fresh martensite is a HE susceptible phase, which is, together with the application of stress, very prone to hydrogen induced cracking. However, also the uncharged condition showed similar tendencies since indeed hydrogen was already present in the retained austenite during the processing of the steel. Additional electrochemical hydrogen charging caused a ductility loss since the ferrite matrix lost its crack arresting ability to absorb hydrogen from the supersaturated transformation induced fresh martensite. The crack initiation site was hence not modified by electrochemical hydrogen charging, while further crack propagation did accelerate when the material was charged with hydrogen. Similar tendencies were observed for TRIP 0% and TRIP 15%, evidencing the proposed failure mechanism. Although indeed the major part of austenite had already transformed to martensite before tensile testing for TRIP 15%, still crack initiation was detected at these martensitic regions due to the rather large amount of hydrogen present at the retained austenite, as demonstrated in Figure 5 (b). Consequently, when hydrogen containing retained austenite is present, crack initiation is triggered over there during tensile testing as it transforms to fresh martensite.

This crack initiation mechanism is supported by many studies [21, 38, 53, 54, 55]. Hydrogen induced cracking was for instance evaluated by EBSD in [56], where cracks were also found to be initiated in martensite, which was freshly transformed from the unstable austenite, and propagated into the adjacent ferrite. Ryu et al. [57] studied the impact of deformation on the hydrogen interaction with TRIP steels regarding their hydrogen trapping and effusion characteristics. Plastic deformation caused the transformation from austenite to martensite and modified the inherited trapped hydrogen. Since austenite has a reasonably larger solubility for hydrogen than ferrite and

martensite, the deformation induced martensitic transformation induces a reduction of trap binding energy and an increased mobility, which results in accelerated failure [57].

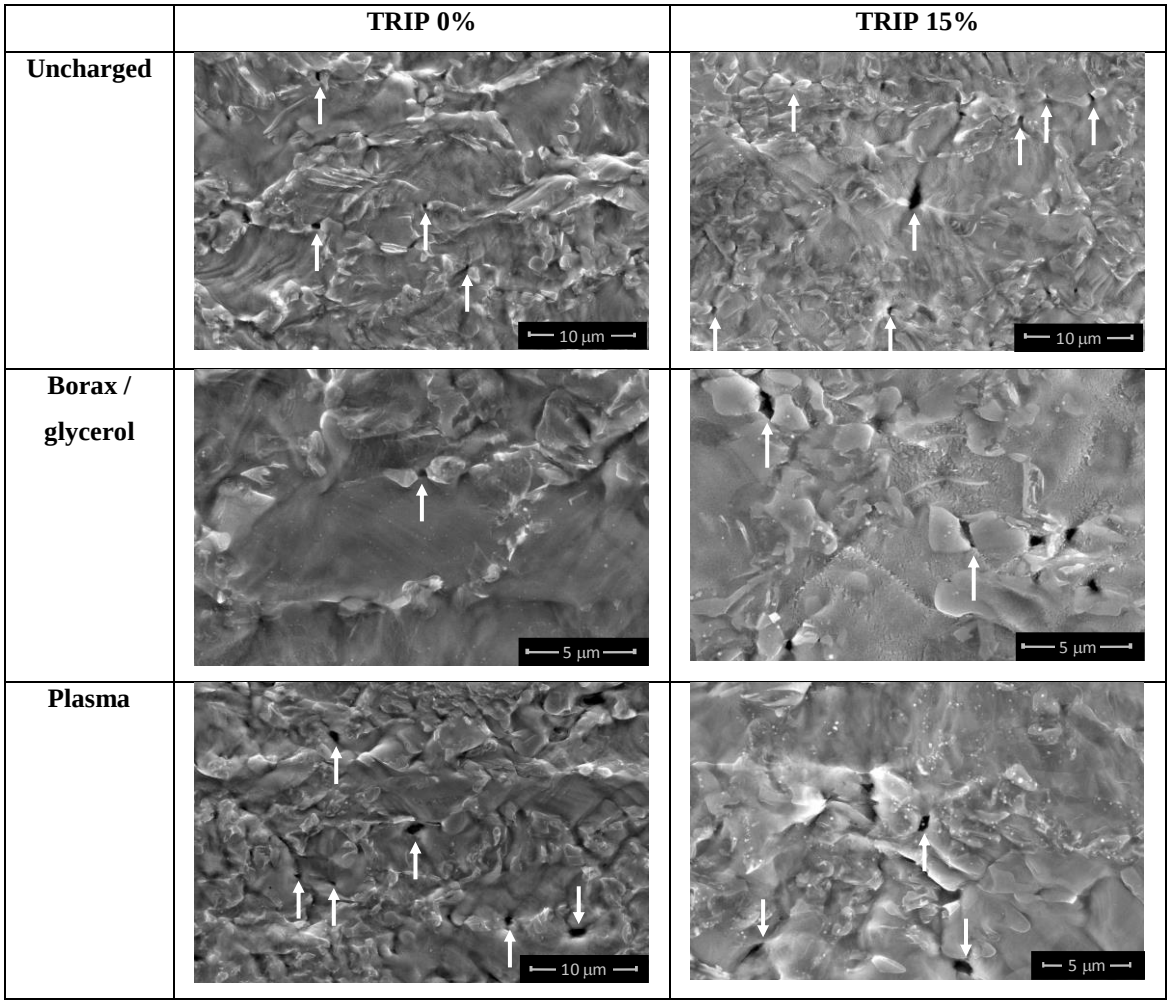

Figure 6: Detailed ESEM images indicating the cracking initiation sites by white arrows for TRIP 0% and TRIP 15% in the uncharged, electrochemical charged and hydrogen plasma charged condition.

When considering the hydrogen plasma charged condition, a different microstructural crack initiation site was found, as observed from Figure 6 and indicated by the white arrows. Crack initiation was mainly detected inside the ferrite matrix. Moreover, since plasma charging resulted in a ductility enhancement compared to the uncharged condition (cf. Figure 4), this observation might account for the observed HE degrees (cf. Table 3). Crack initiation in the soft crack arresting ferrite compared to crack initiation in the brittle martensitic phase can result in the observed increased material' ductility. However, since crack initiation usually occurs at the martensite/martensite interface in this material, further analysis needs to be done on the hydrogen-related characteristics of the retained austenite during tensile testing when plasma charged.

7. Effect of hydrogen plasma on deformation induced phase transformation

The TDS spectra of TRIP 0% and TRIP 15% (cf. Figure 5 (b)) revealed the presence of hydrogen at retained austenite. The high temperature TDS peaks were also present without hydrogen charging, as they originate from the processing [18]. Hence, the retained austenite in the uncharged condition also contains hydrogen, responsible for crack initiation at martensite/martensite interfaces. To comprehend the different crack initiation when plasma

charging was done, complementary TDS measurements were done to verify the effect of plasma on the transformation from austenite to martensite during micro-mechanical tensile testing. Therefore, tensile specimens of TRIP 0% were 20% strained at 10^{-4} s^{-1}, i.e. just before necking (cf. Figure 4), in the uncharged and the in-situ plasma charged condition under an identical vacuum. The gauge section, which underwent the deformation, was then taken for TDS analysis. Time was given to the sample for hydrogen to effuse from the low temperature peak (cf. Figure 5(b)), since the focus lied on the effect of in-situ plasma charging on the deformation induced transformation of austenite to martensite, represented by the high temperature peak in the TDS profile. Corresponding results are shown in Figure 7. Less hydrogen was present for the specimen which was deformed till 20% during in-situ plasma charging (0.38 ± 0.02 wppm hydrogen) compared to the uncharged condition (1.93 ± 0.05 wppm hydrogen), indicating that the fraction of austenite decreased more during deformation in the plasma.

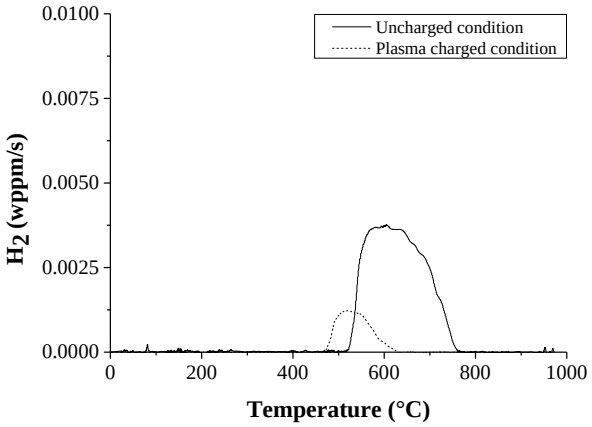

Figure 7: TDS spectra for 20% tensile strained samples in uncharged and plasma charged condition.

Less hydrogen was present for the specimen which was deformed till 20% during in-situ plasma charging compared to the uncharged condition, indicating that the fraction of austenite decreased more during deformation in the plasma. To verify whether plasma charging caused an accelerated transformation to martensite, three complementary EBSD analysis were done for each condition after tensile straining to 20%. The representative phase maps, presented in Figure 8, show that significantly less austenite was present for the sample which was tensile strained during plasma charging, i.e. 1.3% ± 0.3 compared to 3.4% ± 0.4 for the uncharged condition. This observation is in good agreement with the EBSD work performed by Claeys et al. [19], demonstrating the effect of hydrogen on the transformation behaviour in austenite-containing materials during tensile straining. These numbers are in good agreement when compared with the peak areas in the TDS measurements of Figure 5 (b) and the corresponding austenite fraction for the TRIP 0% and TRIP 15% material. Consequently, in-situ plasma charging increased the kinetics of the strain induced phase transformation. This phase transformation can be correlated to the stacking fault energy of the austenite, since low stacking fault energy (< 20 mJ/m^2) favors the martensitic phase transformation [58]. The observed difference in martensite transformation kinetics can be associated to the effect of the hydrogen plasma on the stacking fault energy of the material.

Hydrogen has been suggested to decrease the stacking fault energy, hence favouring the transformation from austenite to martensite. Whiteman and Troiano [59] detected a more faulted structure in a hydrogen charged austenitic stainless steel, while Hermida et al. [60] observed an increasing amount of ε-martensite with increasing cold reduction in hydrogen charged austenitic stainless steel. However, no direct comparison was made between uncharged and hydrogen charged material. Furthermore, Pontini et al. [61] found a 37% reduction in stacking fault

energy by XRD in AISI 304 austenitic stainless steel, while Robertson [62] measured a 20% reduction by in-situ TEM in AISI 310 austenitic stainless steel, both after hydrogen charging. Recently, a direct observation of hydrogen-enhanced martensitic transformation in a duplex stainless steel was found by Claeys et al. [19] by direct comparison of uncharged and hydrogen charged samples. The increased amount of hexagonal close packed (hcp) ε- and body centred tetragonal (bct) α-martensite was confirmed by EBSD analysis following in-situ hydrogen tensile testing. The direct transformation of retained austenite in this TRIP-assisted steel to the bct α-martensite can be explained by a too high strain level at which the tensile test was stopped and at which the intermediate epsilon-phase had already disappeared. Alternatively, H decreased the distance between partial dislocations in pile-ups. These partial dislocations cannot recombine and cross-slip when the SFE is sufficiently reduced, e.g. by hydrogen. It is stated that the core of the slightly separated partial dislocations in the pile-up is close to the BCC stacking. Such an α'-martensite embryo is stabilised faster in the presence of hydrogen due to the reduced distance between the partials [63]. Therefore, the intermediate transformation to ε-martensite might not be a prerequisite while the SFE reduction assists this phenomenon.

During the tensile deformation, the unstable austenite was made less stable by the presence of hydrogen, which induced further martensite transformation [64]. In-situ hydrogen plasma charging, which continued during the deformation, thus induced a faster transformation upon tensile testing, resulting in no more hydrogen containing austenite from the necking point onwards where crack initiation occurred. Moreover, this faster formation of martensite in TRIP steel enhanced the tensile elongation due to retardation of local necking, according to [65]. In addition, for the plasma condition, crack initiation occurred in ferrite leading to an improved toughness due to the crack arresting characteristics of the ferritic matrix.

Furthermore, an increased yield strength and stress flow level can be detected for the in-situ plasma charged samples compared to the other conditions, as shown in Figure 4. The work hardening rate is hence in the early stages of deformation increased by the presence of hydrogen, which is continuously applied during the in-situ hydrogen plasma tensile testing. This can be understood from the faster transformation to hard martensite in the case of in-situ plasma charging.

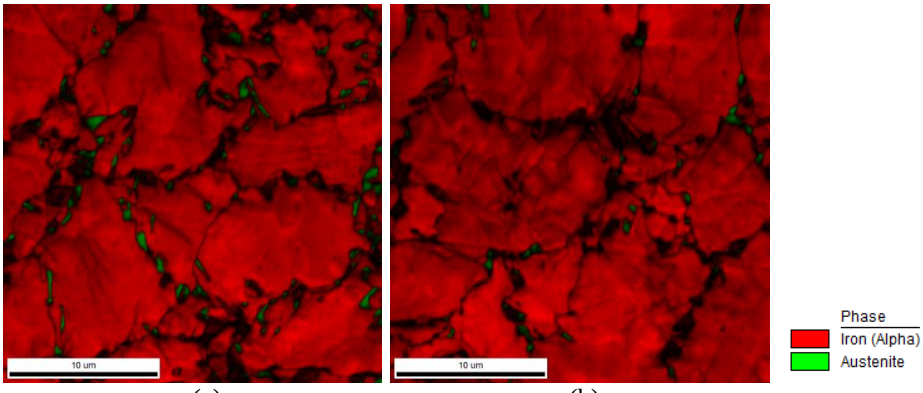

(a) (b)

Figure 8: SEM-EBSD analysis showing the phase maps of the samples after tensile straining to 20% in the uncharged (a) and in-situ hydrogen plasma charged (b) condition.

8. Conclusion

The present study evaluates the hydrogen embrittlement sensitivity and related hydrogen assisted crack initiation by in-situ hydrogen plasma charging in transformation induced plasticity (TRIP) steel. Cold deformation of 15% is performed on the material to induce, on the one hand, defects such as dislocations, and on the other hand, a deformation induced phase transformation from retained austenite to martensite. The susceptibility to hydrogen embrittlement is hence evaluated in two material conditions, i.e. TRIP 0% and TRIP 15%. Hydrogen plasma charging is compared with conventional electrochemical cathodic charging, while uncharged tensile samples serve as a reference.

- A hydrogen induced ductility loss is found when the samples are charged electrochemically with hydrogen, whereas plasma charging remarkably causes a ductility increase for both TRIP 0% and TRIP 15%. Both the yield strength as the flow stress increased when hydrogen charging was applied.
- A comprehensive hydrogen assisted crack analysis by ESEM revealed that the uncharged and electrochemically charged specimens show crack initiation in the martensitic regions. On the contrary, plasma charging resulted into crack initiation in the soft arresting ferritic matrix, accounting for the found engineering stress-strain behavior.
- This was correlated to the effect of in-situ hydrogen plasma charging on the stacking fault energy of austenite. This caused a faster phase transformation upon tensile testing during plasma charging, as verified by combined SEM-EBSD and TDS analysis after tensile straining to 20%.
- Generally, the hydrogen effect is for both charging conditions more pronounced when cold deformation was applied, which is correlated to hydrogen trapping ability of the deformation induced defects. This was demonstrated by thermal desorption spectroscopy, which revealed increased hydrogen trapping with higher dislocation density.

Acknowledgements

TD holds a postdoctoral fellowship via the Research Foundation – Flanders (FWO, grant 12ZO420N). The authors also wish to thank the Special Research Fund (BOF), UGent (BOF15/BAS/062 and BOF01P03516). The authors also acknowledge the technicians and staff working at the Department Materials, Textiles and Chemical Engineering, UGent, for their help with the experiments and/or sample preparation. DW, DW and AB acknowledge the HyF-Lex project founded by RCN (Project No.: 244068/E30).

Data availability

The raw/processed data required to reproduce these findings cannot be shared at this time as the data also forms part of an ongoing study.

References

[1] Martin ML, Somerday BP, Ritchie RO, Sofronis P, Robertson IM, „Hydrogen-induced intergranular failure in nickel revisited," *Acta Mat,* vol. 60, pp. 2739-2745, 2012.

[2] Robertson IM, Sofronis P, Nagao A, Martin ML, Wang S, Gross DW, Nygren KE, „HE understood," *Met Mat Trans B,* vol. 46, pp. 1085-1103, 2015.

[3] Depover T, Pérez Escobar D, Wallaert E, Zermout Z, Verbeken K, „Effect of in-situ hydrogen charging on the mechanical properties of advanced high strength steels," *Int Journal of Hydrogen Energy,* vol. 39, pp. 4647-4656, 2014.

[4] Nygren K, Wang S, Bertsch K, Bei H, Nagao A, Robertson I, „Hydrogen embrittlement of the equi-molar FeNiCoCr alloy," *Acta Mat,* vol. 157, pp. 218-227, 2018.

[5] Koyama M, Akiyama E, Lee Y-K, Raabe D, Tsuzaki K, „Overview of hydrogen embrittlement in high-Mn steels," *International Journal of Hydrogen Energy,* vol. 42, pp. 12706-12723, 2017.

[6] Brandon NP, Kurban Z, „Clean energy and the hydrogen economy," *Phil Trans R Soc A,* vol. 375: 20160400, 2017.

[7] Ad van Wijk, „Green Hydrogen Economy in the Northern Netherlands," The Nothern Netherlands Innovation Board, Groningen, 2017.

[8] „https://www.h21.green/," [Online]. Available: https://www.h21.green/.

[9] Loidl M, Kolk O, „Hydrogen embrittlement in HSSs limits use in lightweight body," *Advanced Materials and Processes,* vol. 169, pp. 22-25, 2011, BMW Group, Germany.

[10] Depover T, Wallaert E, Verbeken K, „Fractographic analysis of the role of hydrogen diffusion on the hydrogen embrittlement susceptibilty of DP steel," *Mat Sci and Eng A,* vol. 649, pp. 201-208, 2016.

[11] Laureys A, Depover T, Petrov R, Verbeken K, „Characterization of hydrogen induced cracking in TRIP-assisted steels," *Int Journal of Hydrogen Energy,* vol. 40, nr. 47, pp. 16901-16912, 2015.

[12] Laureys A, Depover T, Petrov R, Verbeken K, „Microstructural characterization of hydrogen induced cracking in TRIP-assisted steel by EBSD," *Materials Characterization,* vol. 112, pp. 169-179, 2016.

[13] Laureys A, Pinson M, Depover T, Petrov R, Verbeken K, „EBSD characterization of hydrogen induced blisters and internal cracks in," *Materials Characterization,* vol. 159, 2020, 110029.

[14] De Cooman BC, „Structure–properties relationship in TRIP steels containing carbide-free bainite," *Curr Opin Solid State Mater. Sci,* vol. 8, pp. 285-303, 2004.

[15] Kiuchi K, McLellan RB, „The solubility and diffusivity of hydrogen in well-annealed and deformed iron," *Acta Metall,* vol. 31, pp. 961-984, 1983.

[16] Olden V, Thaulow C, Johnsen R , „Modelling of hydrogen diffusion and hydrogen induced cracking in supermartensitic and duplex stainless steels," *Mater Des,* vol. 29, p. 1934–1948, 2008.

[17] Van den Eeckhout E, I De Baere, Depover T, Verbeken K, „The effect of a constant tensile load on the hydrogen diffusivity in dual phase steel by electrochemical permeation experiments," *Mat Sci and Eng A,* vol. 733, 2020, 138872.

[18] Pérez Escobar D, Depover T, Wallaert E, Duprez L, Verbeken K, Verhaege M, „Combined thermal desorption spectroscopy, differential scanning calorimetry, scanning electron microscopy and X-ray diffraction study of hydrogen trapping in cold deformed TRIP steel," *Acta Mat,* vol. 60, pp. 2593-2605, 2012.

[19] Claeys L, Depover T, De Graeve I, Verbeken K, „First observation by EBSD of martensitic transformations due to hydrogen presence during straining of duplex stainless steel," *Mat Char,* vol. 156, p. 109843, 2019.

[20] Wang D, Lu X, Wan D, Zhiming L, Barnoush A, „In-situ observation of martensitic transformation in an interstitial metastable high-entropy alloy during cathodic hydrogen charging," *Scripta Mat,* vol. 173, pp. 56-60, 2019.

[21] McCoy RA, Gerberich WW, „Hydrogen embrittlement studies of a TRIP steel," *Metallurgical Transactions,* vol. 4, pp. 539-547, 1973.

[22] Chan SLI, „Hydrogen trapping ability of steelswith differentmicrostructures," *J Chin Inst Eng,* vol. 22, pp. 43-53, 1999.

[23] Depover T, Verbeken K, „The detrimental effect of mobile hydrogen at dislocations on the hydrogen embrittlement susceptibility of Fe-C-X alloys: an experimental proof of the HELP mechanism," *Int Journal of H Energy,* vol. 43, pp. 3050-3061, 2018.

[24] Nagao A, Dadfarnia M, Somerday B, Sofronis P, O. Ritchie R, „Hydrogen-enhanced-plasticity mediated decohesion for hydrogen-induced intergranular and "quasi-cleavage"fracture of lath martensitic steels," *Journal of the mechanics and physics of solids,* vol. 112, pp. 403-430, 2018.

[25] Dadfarnia M, Martin ML, Nagao A, Sofronis P, Robertson IM, „Modeling hydrogen transport by dislocations," *Journal of the Mechanics and Physics of Solids,* vol. 78, pp. 511-525, 2015.

[26] Leyson GPM, Grabowski B, Neugebauer J, „Multiscale modeling of hydrogen enhanced homogeneous dislocation nucleation," *Acta Mat,* vol. 107, pp. 144-151, 2016.

[27] Venezuela J, Tapia-Bastidas C, Zhou Q, Depover T, Verbeken K, Gray E, Liu Q, Liu Q, Zhang M, Atrens A, „Determination of the equivalent hydrogen fugacity during electrochemical charging of 3.5NiCrMoV steel," *Corrosion Science,* vol. 132, pp. 90-106, 2018.

[28] Atrens A, Venezuela J, Liu Q, Zhou Q, Verbeken K, Tapia-Bastidas C, Gray E, Christien F, Wolski K, „Electrochemical and mechanical aspects of hydrogen embrittlement evaluation of martensitic steels," *Surface Science and Electrochemistry,* pp. 201-225, 2018.

[29] Barnoush A, Vehoff H, „Recent developments in the study of hydrogen embrittlement: Hydrogen effect on dislocation nucleation," *Acta Mat,* vol. 58, pp. 5274-5285, 2010.

[30] Wang D, Lu X, Deng Y, Guo X, Barnoush A, „Effect of hydrogen on nanomechanical properties in Fe22Mn-0.6C TWIP steel revealed by in-situ electrochemical nanoindentation," *Acta Mat,* 2019, doi.org/10.1016/j.actamat.2018.12.055.

[31] Claeys L, Cnockaert V, Depover T, De Graeve I, Verbeken K, „Critical assessment of the evaluation of thermal desorption spectroscopydata for duplex stainless steels: A combined experimental and numerical approach," *Acta Mat,* vol. 186, pp. 1-9, 2020.

[32] Yamabe J, Takakuwa O, Matsunaga H, Itoga H, Matsuoka S, „Hydrogen diffusivity and tensile-ductility loss of solution-treated austenitic stainless steels with external and internal hydrogen," *Int Journal of Hydrogen Energy,* vol. 42, pp. 13289-13299, 2017.

[33] Ichii K, Koyama M, Tasan CC, Tsuzaki K, „Comparative study of hydrogen embrittlement in stable and metastable high-entropy alloys," *Scripta Mat,* vol. 150, pp. 74-77, 2018.

[34] Koyama M, Akiyama E, Lee YK, Raabe D, Tsuzaki K, „Overview of hydrogen embrittlement in high-Mn steels," *Int Journal of Hydrogen Energy,* vol. 42, pp. 12706-12723, 2017.

[35] Dadfarnia M, Sofronis P, Somerday BP, Balch DK, Schembri P, Melcher R, „On the environmental similitude for fracture in the SENT specimen and a cracked hydrogen gas pipeline," *Engineering Fracture Mechanics,* vol. 78, pp. 2429-2438, 2011.

[36] Wan D, Deng Y, Barnoush A, „Hydrogen embrittlement effect observed by in-situ hydrogen plasma charging on a ferritic alloy," *Scripta Mat,* vol. 151, pp. 24-27, 2018.

[37] Depover T, Hajilou T, Wan D, Wang D, Barnoush A, Verbeken K, „Assessment of the potential of hydrogen plasma charging as compared to conventional electrochemical hydrogen charging on dual phase steel," *Mat Sci and Eng A,* vol. 754, pp. 613-621, 2019.

[38] Ronevich JA, Speer JG, Matlock DK, „Hydrogen embrittlement of commercially produced advanced high strength sheet steels," *SAE Int J Mater Manuf,* vol. 3, pp. 255-267, 2010.

[39] Hajilou T, Hope MSB, Zavieh A, Kheradmand N, Johnsen R, Barnoush A, „In situ small-scale hydrogen embrittlement testing made easy: An electrolyte for preserving surface integrity at nano-scale during hydrogen charging"," *Int Journal of Hydrogen Energy,* vol. 43, pp. 12516-12529, 2018.

[40] Lee JY, Lee SM, „Hydrogen trapping phenomena in metals with bcc and fcc crystal structures by the desorption thermal-analysis technique," *Surface and Coatings Technology,* vol. 28, pp. 301-314, 1986.

[41] Kissinger HE, „Reaction kinetics in differential thermal analysis," *Analytical Chemistry,* vol. 29, pp. 1702-1706, 1957.

[42] Depover T, Wallaert E, Verbeken K, „On the synergy of diffusible hydrogen content and hydrogen diffusivity in the mechanical degradation of laboratory cast Fe-C alloys," *Mat Sci and Eng A,* vol. 664, pp. 195-205, 2016.

[43] Depover T, Vercruysse F, Elmahdy A, Verleysen P, Verbeken K, „Evaluation of the hydrogen embrittlement susceptibility in DP steel under static and dynamic tensile conditions," *International Journal of Impact Engineering,* vol. 123, pp. 118-125, 2019.

[44] Wagih M, Tang Y, Hatem T, El-Awady JA, „Discerning enhanced dislocation plasticity in hydrogen-charged α-iron nano-crystals," *Materials Research Letters,* vol. 3, pp. 184-189, 2015.

[45] Murakami Y, Kanezaki T, Mine Y, „Hydrogen effects against hydrogen embrittlement," *Met Mat Trans A,* vol. 41, pp. 2548-2562, 2010.

[46] Kirchheim R, „Solid solution softening and hardening by mobile solute atoms with special focus on hydrogen," *Scripta Mat,* vol. 67, pp. 767-770, 2012.

[47] Luo H, Li Z, Lu W, Ponge D, Raabe D, „Hydrogen embrittlement of an interstitial equimolar high-entropy alloy," *Corrosion Science,* vol. 136, pp. 403-408, 2018.

[48] Hirth JP, „Effects of Hydrogen on the Properties of Iron and Steel," *Met Trans A,* vol. 11A, pp. 861-890, 1980.

[49] Presouyre GM, „Classification of hydrogen trapping in steel," *Met Trans A,* vol. 10A, pp. 1571-1573, 1979.

[50] Thomas LSR, Li D, Gangloff RP, Scully JR, „Trap-governed hydrogen diffusivity and uptake capacity in ultrahigh strength aermet 100 steel," *Met Mat Trans A,* vol. 33A, pp. 1991-2004, 2002.

[51] Depover T, Verbeken K, „The effect of TiC on the hydrogen induced ductility loss and trapping behavior of Fe-C-Ti alloys," *Corrosion Science,* vol. 112, pp. 308-326, 2016.

[52] Depover T, Verbeken K, „Evaluation of the role of Mo2C in hydrogen induced ductility loss in Q&T Fe-C-Mo alloys," *Int Journal of Hydrogen Energy,* vol. 41, pp. 14310-14329, 2016.

[53] Ronevich J, De Cooman B, Speer J, De Moor E, Matlock D, „Hydrogen effects in prestrained transformation induced plasticity steel," *Metall Mater Trans A,* vol. 43, pp. 2293-2301, 2012.

[54] Loidl M, Kolk O, Veith S, Göbel T, „Characterization of hydrogen embrittlement in automotive advanced high strength steels," *Mater Sci Eng Technol,* vol. 42, pp. 1105-110, 2011.

[55] Imlau J, Bleck W, Zaefferer S, „Comparison of damage development depending on the local microstructure in low alloyed Al-TRIP-steels, IF steel and a DP steel," *Int J Mater Res,* vol. 100, pp. 584-593, 2009.

[56] Zhu X, Li W, Zhao H, Jin X, „Effects of cryogenic and tempered treatment on the hydrogen embrittlement susceptibility of TRIP-780 steels," *Int J Hydrogen Energy,* vol. 38, pp. 10694-10703, 2013.

[57] Ryu JH, Chun YS, Lee CS, Bhadeshia HKDH, Suh DW, „Effect of deformation on hydrogen trapping and effusion in TRIP-assisted steel," *Acta Mater,* vol. 60, pp. 4085-4092, 2012.

[58] Sato K, Ichinose M, Hirotsu Y, Inoue Y , „Effects of deformation induced phase transformation and twinning on the mechanical properties of austenitic Fe-Mn-Al alloys," *ISIJ Int,* vol. 29, pp. 868-877, 1989.

[59] Whiteman MB, Troiano AR, „The Influence of Hydrogen on the Stacking Fault Energy of an Austenitic Stainless Steel," *Physica Status Solidi,* vol. 7, pp. 109-110, 1964.

[60] Hermida JD, Roviglione A, „Stacking fault energy decrease in austenitic stainless steels induced by hydrogen pairs formation," *Scripta materialia,* vol. 38, nr. 8, pp. 1145-1149, 1998.

[61] Pontini AE, Hermida JD, „X-ray diffraction measurement of the stacking fault energy reduction induced by hydrogen in an AISI 304 steel," *Scripta materialia,* vol. 37, nr. 11, pp. 1831-1837, 1997.

[62] Robertson IM, „The effect of hydrogen on dislocation dynamics," *Engineering fracture mechanics,* vol. 64, pp. 649-673, 1999.

[63] Brooks J, Loretto M, Smallman R, „Direct observations of martensite nuclei in stainless steel," *Acta Metall,* vol. 27, pp. 1839-1847, 1979.

[64] Liu Q, Zhou Q, Venezuela J, Zhang M, Wang J, Atrens A, „A review of the influence of hydrogen on the mechanical properties of DP, TRIP, and TWIP advanced high-strength steels for auto construction," *Corros Rev,* vol. 34, pp. 127-152, 2016.

[65] Grässel O, Krüger L, Frommeyer G, Meyer LW, „High strength Fe-Mn-(Al, Si) TRIP/TWIP steels development - properties - application," *International Journal of Plasticity*, vol. 16, pp. 1391-1409, 2000.